COMPUTER SIMULATION OF THE FLOWPATH IN MAGNETIC SEALLESS PUMPS

by

Adiel Guinzburg

Rotating Machinery Analyst

Rocketdyne Division, Boeing North America

Canoga Park, California

and

Frederic W. Buse

Senior Engineering Consultant

Ingersoll-Dresser Pump Company

Phillipsburg, New Jersey

Adiel Guinzburg is a Rotating Machinery Analyst at the Rocketdyne Division of Boeing North America, Incorporated, in Canoga Park, California. She was previously a Staff Researcher at Ingersoll-Dresser Pump Company, where she conducted research on a variety of industrial pumps and components. Prior to that, she was a Research Scientist at the Institut de Machines Hydrauliques et de Mécaniques des fluides at the Ecole Polytechnique Féderale de Lausanne, Switzerland.

Dr. Guinzburg received a B.Sc degree (Aeronautical Engineering) from the University of the Witwatersrand (1985), an M.S. degree (Aeronautics) from the California Institute of Technology (1986), and a Ph.D. degree from the California Institute of Technology (1991). She is a member of AIAA and ASME, having served as Subcommittee Chair for Fluid Machinery and as an editor for the Third International Symposium on Pumping Machinery. Dr. Guinzburg is currently Vice-Chair for the Fluids Applications and Systems Technical Committee of ASME. She has authored several technical papers.

Frederic W. Buse is a Senior Engineering Consultant at Ingersoll-Dresser Pump Company in Phillipsburg, New Jersey, where he has been employed for 39 years.

Mr. Buse is a member of the Hydraulic Institute and of ANSI Committees B73.1 and B73.2. He has contributed to Marks' Standard Handbook for Mechanical Engineers, *the* Pump Handbook, *and* Pump Application and Design. *He has written numerous articles and has received 20 U.S. patents on centrifugal and reciprocating pumps. He has contributed to API specifications for reciprocating pumps and has also contributed to the ASME test code on centrifugal pumps. Mr. Buse represents the United States for writing the ISO centrifugal pump standards. He is chairman of several Hydraulic Institute Committees. He has also been author and coauthor of several papers and tutorials for the International Pump Users Symposia.*

Mr. Buse is a graduate of New York Maritime College, with a B.S. degree (Marine Engineering).

ABSTRACT

For applications that involved fluids with a high rate of change of vapor pressure or low specific heat, it was found that there could be inadequate flow through the thrust bearing. This effect was compounded by the heat generation due to the eddy currents that occur in magnetic drive pumps with metallic shells.

This paper describes a *computer simulation* to predict the flows, pressures, and temperatures in magnetic drive sealless pumps. The program has been developed using both theoretical and test work. The objective of the program was to provide reliable selection of magnetic drive pumps; this was accomplished by taking into account the effects of viscosity, vapor pressure, and other liquid properties on the local pressures in the pump.

The goal of this program was thus to simulate a customer's desired application of a particular fluid at an operating pressure, temperature, NPSH, and speed. The resulting conclusion would be whether the customer's fluid and operating conditions were applicable for sealless pumps. *Warnings* are output through the graphical user interface of the program at the various points, should flashing occur using the particular fluid.

The testing involved a wide range of pump sizes. Within each size, an extensive matrix involved running at different speeds, different cut impeller diameters, and from shutoff through runout condition. The units were tested with different shell configurations and different materials. These included polyetheretherketone (known as PEEK), Alloy C-276, and a dual containment consisting of both materials.

The design of the back shroud influences the magnitude of the hub factor. This is because the traditional affinity laws cannot be applied to the calculation of the axial load for a semiopen impeller with a scalloped back shroud, pump out vanes, or pump out slots. One of the important findings was that the impeller hub factor, which is required for the computation of the axial load, changed as a function of speed and cut impeller diameter. It was also found that pump out vanes or pump out slots significantly enhanced the lubrication through the bearings and across the magnets.

Part of the verification involved performing tests with different bushing clearances and grooving configurations. These were analyzed empirically to confirm the coefficients that were obtained from experimental methods.

In order to examine the possible operation of the pump when handling the user's particular fluid, the flow is simulated in the program using a graphical user interface. A graphical output is given of all the pertinent locations in the system, such as the thrust collar face or the gap between the driven magnets and the shell.

The program currently calculates the pressure, flow, and temperature within the flowpath, along with the axial thrust, at five pump operating flow conditions expressed as a percentage of the best efficiency point.

INTRODUCTION

In recent years, the increasing emphasis on the prevention of leakage of process fluids in many areas of application has led to the introduction of sealless pumps (Buse and Stoughton, 1990; Hernandez, 1991; Mayes, 1990; and Schommer and Johnson, 1990). Some of these are canned motor pumps and others are driven through a magnetic coupling by a standard motor. This paper focuses on the latter type. The purpose of a sealless pump is to replace a shaft that penetrates into the atmosphere, and to directly drive the impeller. A magnetically driven sealless pump has a sealed containment shell, thereby driving internal magnets on a shaft that has an impeller attached to it. Sealless pumps have been avoided by some users in light hydrocarbon services for two main reasons. Light hydrocarbons tend to flash very easily. Also, light hydrocarbons tend to have very poor lubricating properties.

The concept of magnetically coupled pumps has been introduced in previous pump users symposia (Buse and Stoughton, 1990; Hernandez, 1991; Mayes, 1990; and Schommer and Johnson, 1990). It has also been shown that construction details that have caused problems in the past can be resolved by innovative applications of new and emerging technologies (Heald, et al., 1992).

Magnetically coupled pump technology has seen the use of innovative designs, materials, and application techniques. The power transmitted has increased, while increasing the drive efficiency (Mayes, 1990).

Magnetic drive pumps were reintroduced as a viable alternative to sealed pumps in 1987 to 1989. Because of the development of rare earth magnetic materials and silicon carbide bearings, magnetic drive pumps dominated the scene.

PUMP CONFIGURATION

This paper describes a program to predict the flows, pressures, and temperatures in magnetic drive sealless pumps (Figure 1). The magnetically driven sealless pumps for which this simulation was developed had semiopen impellers in an end-suction, single-volute configuration. The impellers are scalloped and have either pump out vanes (Figure 2) or pump out slots to reduce the axial load. The pump also had a containment shell that could be either metallic, nonmetallic, or dual containment, which is a combination of both.

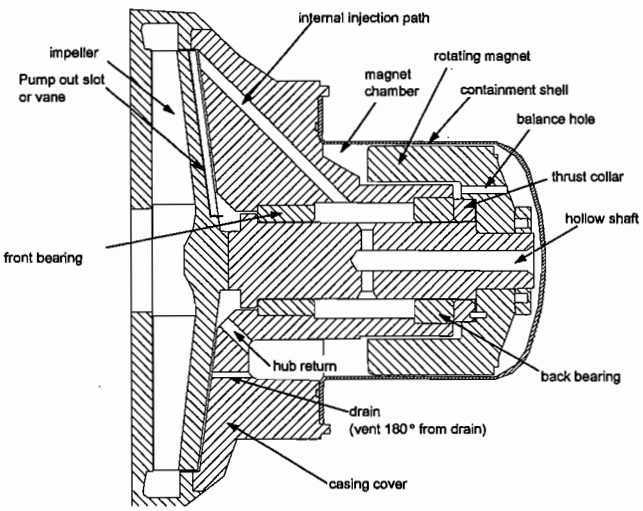

Figure 1. Magnetic Sealless Pump Components for the Internal Flow System.

Figure 2. Typical Semiopen Impeller with a Scalloped Shroud and Pump Out Vanes on the Rear of the Shroud.

FLOWPATH

Inside the sealless pump is a complex internal flow system that is crucial to the successful operation of this type of machine, due to the need to effectively cool the magnetic drive and lubricate the bearings. With low specific heat volatile liquids, it is important to be able to predict flashing, which could result in premature pump failure.

The containment shell, installed between the inner driven and outer drive magnets, prevents the internal flow from leaking to the atmosphere. When this shell is made of a conductive material, it will generate eddy currents. The eddy current losses in the shell generate heat, which will consume 10 to 20 percent of the pump horsepower. For example, when using a metallic shell, the eddy currents can cause the temperature of the lubricating fluid to increase by 0.3°F to 10°F, which can result in the flashing of the pump fluid and therefore pump damage. In order to conduct this heat away and to avoid vaporizing in the shroud area, a certain flow through the gap between internal rotor and shell is required. Most magnetically coupled pump designs use the pumped liquid to lubricate the bearings and to cool the area surrounding the magnets. A portion of the heat is removed from the internal flow of the liquid through the lubrication system. Both the thrust and radial bearings are lubricated by the pumped fluid, which is required to avoid failure. The internal circulation in the various portions of the flowpath of a typical pump model is shown in Figure 3 and Table 1. It can be seen that in this particular flowpath, the fluid does not return to the suction of the impeller. The circulation (Q_f) starts from behind the impeller and enters between the bearings. The flow splits into three portions where one portion goes through the back bearings (Q_{bb}). Another portion of the fluid goes down the center of the shaft (Q_s) to the rear of the containment shell and across the magnets (Q_m), and then between the inner rotor and containment shell. Then it goes to the impeller hub (Q_h) to return to the impeller discharge. The third portion passes through the face of the front bearing (Q_{fb}), returning to the impeller hub. The fluid circulates and returns to the impeller discharge after the fluid has removed heat from the bearings and magnetic coupling in the containment shell. Thus, vaporization of the product through temperature rise in the magnet area is inhibited. A small portion of the flow also passes through the vent and drain openings (Q_{vd}). Various investigators conducted tests to determine the pressure at the locations throughout the internal system. Knowledge of the temperature, pressure, and flow of the internal flowpath prevents the occurrence of bearing failures. This paper describes how detailed information of the internal flowpath was obtained experimentally and then coded into a computer program for pressure, flow, and temperature prediction at various locations.

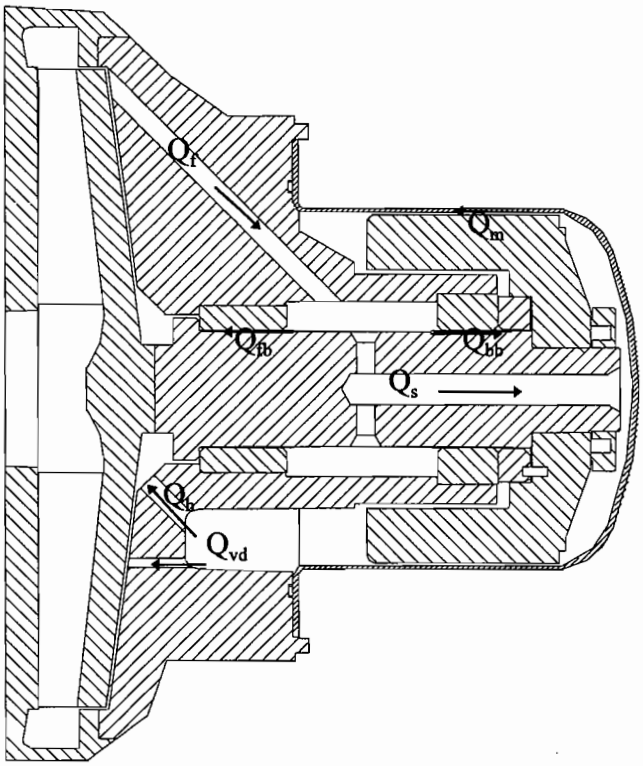

Figure 3. Internal Flow Nomenclature.

Table 1. The Leakage Flows in the Flowpath of a Typical Pump Described in Terms of Pressure Developed.

The leakage flows in the flowpath of a typical pump are described in terms of the pressure developed as follows:
$Q_f = 0.324 \cdot c_q \cdot H^{0.5}$
$Q_{fb} = 0.085 \cdot c_q \cdot H^{0.5}$
$Q_{vd} = 0.079 \cdot c_q \cdot H^{0.5}$
$Q_h = 0.16 \cdot c_q \cdot H^{0.5}$
$Q_f = (Q_{vd} + Q_h + Q_{fb})$
$Q_m = 0.127 \cdot c_q \cdot H^{0.5}$
$Q_s = 0.127 \cdot c_q \cdot H^{0.5}$
$Q_{bb} = (Q_f - Q_{fb} - Q_s)$

The customer's fluid properties, such as specific gravity, vapor pressure, viscosity, and specific heat, are some of the most important elements for successful pump operation. In particular, they affect the bearing life. The fluid specific gravity and viscosity will affect the pump horsepower and developed pressure requirements. Furthermore, the rapid change with temperature of these properties increases the chance of the fluid flashing. For this reason, the slope of the curve of vapor pressure as a function of temperature is extremely critical in the operation of a sealless pump. The higher the rate of change of vapor pressure, the more risk of the fluid flashing with a small increase in temperature; thus the greater risk of fluid flashing in the bearings or around the internal rotor causing temperature rise and wear problems. The fluid viscosity is also important because of the hydrodynamic or frictional losses from the flow in the internal flow passages.

If the fluid pressure approaches the vapor pressure along the flowpath, the fluid could vaporize and cause problems with removing the heat generated by the magnetic coupling. Knowledge of the internal flow is vital to reliable sealless pump operation; hence, the flowrate, pressure, and temperature are given at critical areas.

EXPERIMENTAL MEASUREMENT

To confirm the circulation system, testing was performed with each pump size and with the different combinations of shells. By cross drilling passages in the casing cover, it was possible to access key areas inside the wet end to collect flow, temperature, and static pressure data during pump operation. The experimental setup for pressure measurements is shown in Figure 4.

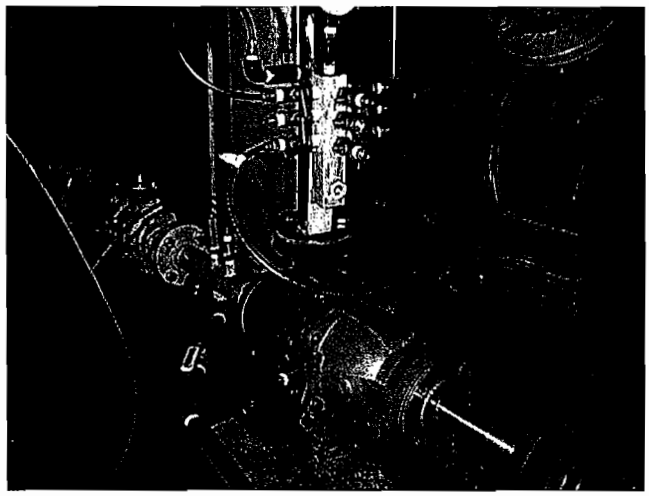

Figure 4. Pressure Measurements.

The results for each passage within the flowpath were then compared with analytical predictions, and adjustments were made to obtain agreement between the two. Pressure and flowrate information for an individual flowpath location (Q_{bb}, Q_{fb}, Q_h, Q_m, Q_s, and Q_{vd}) was obtained by blocking other paths. In some cases, more than one flowpath was investigated at the same time.

In order to obtain the individual flowpath flowrates, an external injection port was drilled into the casing cover and the internal injection path was plugged. In this way, a known artificial leakage flow could be injected and the pressure drop across a particular flowpath could be measured. Pressure measurements were made at various flowrates of the pump. After measurements were made on the individual flowpaths, the pump was run as a unit so that overall measurement of the flowpaths could be made. These pressure readings were compared with the previous tests to determine the flowrate at the various locations.

These data readings were obtained on 14 different sizes of pumps, which included two basic magnet frame sizes nominally 5 hp and 20 hp, four ANSI B 73.1 liquid ends, and 10 ISO liquid ends.

The size of the clearance and the size and number of flush slots in the *front bushing* (Q_{fb}) determines how much flow will pass through the back portion of the flowpath. The vent and drain (Q_{vd}), along with the hub (Q_h) return, were plugged to obtain Q_{fb}. Pressure readings were obtained between the bushings (P_{bb}) and at the impeller hub (P_h) to obtain a pressure drop. Tests were done with a static shaft and with the shaft operating at 1750 and 3550 rpm. The tests showed that there was little difference between the static shaft results and the operating speeds results.

The *vent and the drain* paths (Q_{vd}) were tested as a pair. The hub return (P_h) and the front bushing (P_{bb}) leakage path were plugged. Pressure readings were obtained at the magnet chamber (P_m) and at the exit of the vent and the drain. Results obtained from these measurements also showed no difference between the data obtained with a static shaft and that obtained with the operation of the shaft.

The front bushing, vent, and drain flowpaths were plugged. Pressure readings were obtained at the magnet chamber and the

impeller hub. The size of the *return hole by the impeller hub* (P_h) controls the amount of flow through the back portion of the flowpath and also affects the pressure gradient across the back shroud of the impeller. The optimum amount of flow for cooling is achieved such that the impeller hub pressure is kept low and a low impeller axial load is obtained.

The *internal injection flow* (Q_f) is due to the pressure drop between the impeller peripheral pressure and the pressure between the bearings. The loss at the entrance to the injection path is a combination of loss factors due to turning, swirl, and entrance loses that were difficult to predict empirically.

The front bushing, back bushing, and balance holes in the inner carrier were plugged. Pressure readings were taken at the end of the *shaft hole* (P_{cs}) and compared with readings between the bearings (P_{bb}) to obtain the losses through the shaft. The pressure drop across the magnets was also obtained.

The front bushing and balance holes in the inner carrier were plugged. Pressure readings were obtained between the bushings, at the periphery of the thrust collar (P_{tod}), and in the magnet chamber (P_{mc}). The readings at the back *end of the shell* (P_{bso}) were always higher than at the shaft hole (P_{cs}).

The *thrust collar* has four radial grooves. The pressure at the tip of the thrust collar (P_{tod}) was taken and compared with the pressure between the bushings (P_{bb}) to determine how much pressure was generated by the radial slots. The loss through the back bushing was also taken into account. This was compared with the theoretical gain in pressure from the slots and a favorable comparison was obtained.

VISUAL VERIFICATION

In addition to pressure, temperature, and flow measurements, a clear shell made of polyurethane was used for flow visualization. Tufts of thread were attached to the casing cover, the inside of the shell at the end of the shaft, the end of the magnets, along the magnet length, and by the magnet chamber. In order to observe the flow, the outer carrier was removed. The impeller was reworked so a drive shaft could be attached through the suction nozzle (Figure 5). The pump was run at various speeds and flowrates. The main concern was the direction of flow across the magnets. Since the velocity at the tip of the magnets is much greater than the axial velocity of the flow, the tufts were aligned at a 70 to 80 degree angle to the centerline of the shaft, and were pointing toward the magnet chamber at all flows. The results of the flow visualization are shown in Figure 6. Even with the tufts, it was difficult to observe the direction in which the flow was going at the center of the shaft. To verify the direction of flow further, bright green dye was injected into the external hole while the internal flowpath was being used. This not only verified the direction of the flow through the shaft and out past the magnets, but also allowed for the determination of the transit time for the flow to pass through the system.

VERIFICATION OF THE EXPERIMENTAL RESULTS

The pressure differential across the individual flowpaths when the pump was operated normally was compared with the corresponding differential that was obtained by external flow injection. In this manner the flow through the paths during pump operation was determined.

The experimental setup for the measurement of temperature is shown in Figure 7. After results were obtained for pressure and flow, temperature probes were placed in similar locations to those of the pressure probes. The temperature probes were placed at the pump discharge, the inlet, the impeller hub, between the bearings, and the thrust collar. Measurements were taken at four speeds, with four impeller diameters per pump size using a carbon-reinforced PEEK shell, an Alloy C-276 shell, and a dual combination shell. This was also done with different configurations of the back shroud of the impeller.

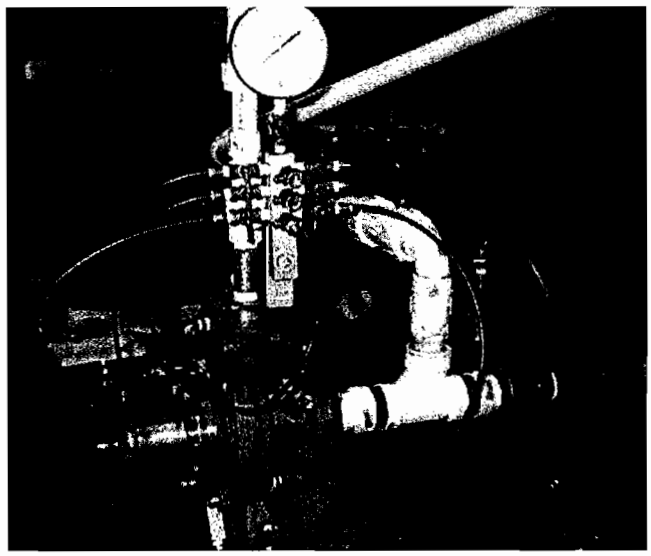

Figure 5. Experimental Setup for Flow Visualization.

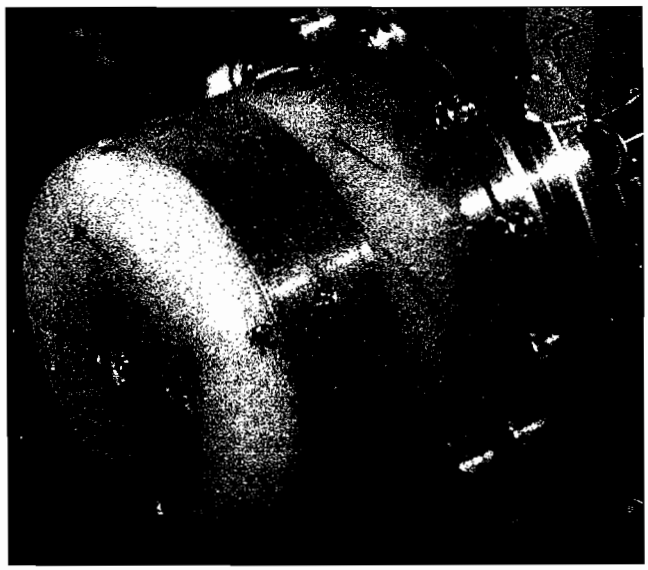

Figure 6. Visualization of the Lubrication Flow Inside the Shell.

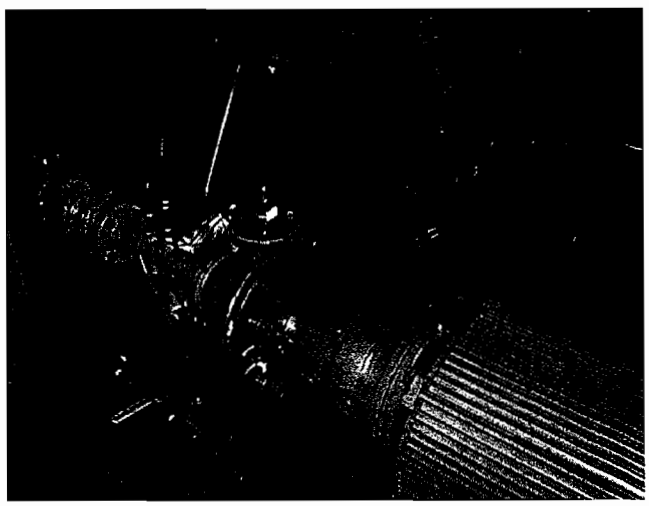

Figure 7. Temperature Measurement.

Using analytical equations and test data, and taking the liquid viscosity, specific gravity, and specific heat into account, a predicted temperature rise across the face of the axial thrust bearing was determined. In the computer program, the user is required to enter the vapor pressure as a function of temperature for the liquid under investigation. Because the testing was done with room temperature water, corrections due to viscosity, which were obtained from Hydraulic Institute Standards, needed to be made. The pressure along the flowpath is compared with the vapor pressure of the liquid at the corresponding temperature. When the local pressure is within 10 percent of the vapor pressure, a *warning signal* is illuminated at the location of this low pressure. The user should then make adjustments to the system to prevent possible problems.

Developed Pressure

From the user's initial selection of pump speed and impeller diameter, the dynamic pressure is calculated. It is in terms of the dynamic pressure given by Equation (2) that the pressures at the various points in the flowpath have been calculated in the program.

$$H \equiv \frac{u^2}{2 \cdot g} \tag{1}$$

$$P \equiv \frac{H \cdot sg}{2.309} \tag{2}$$

The pressures at various locations in the flowpath are shown in Figure 8. (The values of head shown correspond to the flows of the example given in Figure 3, as shown in Table 2.)

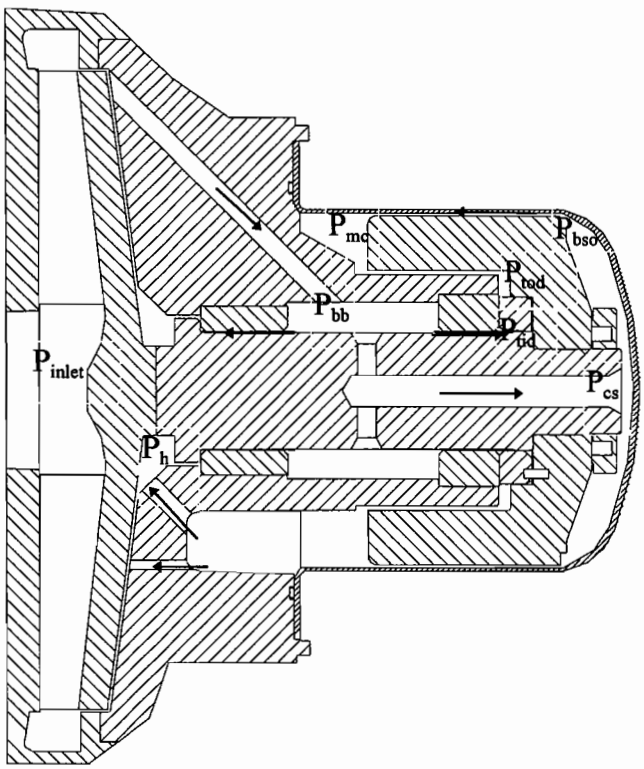

Figure 8. Internal Pressure Nomenclature.

Temperature Calculation

Depending on the amount of load and speed of operation, the face of the thrust collar can be operating in boundary or hydrodynamic lubrication. When in boundary lubrication, a limiting PV value is the acceptance criterion. With hydrodynamic lubrication, the film thickness, which takes the viscosity, temperature, specific gravity, specific heat, and shear stress into account, is the acceptance criterion.

Table 2. Pressure in the Flowpath Expressed as a Ratio of P.

	3%	20%	50%	100%	120%
P_{bb}	0.39	0.36	0.357	0.33	0.27
P_{tod}	0.39	0.36	0.357	0.33	0.27
P_{mc}	0.39	0.34	0.34	0.33	0.27
P_h	0.24	0.22	0.221	0.14	0.06
P_{cs}	0.25	0.23	0.2295	0.21	0.17
P_{bso}	0.31	0.29	0.289	0.26	0.22
P_{tid}	0.31	0.29	0.289	0.22	0.12

In either case, the viscous drag associated with lubrication is expressed as horsepower, which produces a corresponding temperature rise across the thrust face for the amount of liquid passing across the face. The total temperature-pressure is compared to vapor pressure at that temperature.

The components of axial load are impeller load and load from the pressure on the inner magnet carrier caused by circulation of fluid in the containment shell. A study was conducted (Guinzburg and Buse, 1995) to measure the hydraulic loads generated by semiopen impellers. These results were incorporated in the present analysis. The capability of the surface depends on whether there is hydrodynamic or boundary lubrication. It is best to maintain hydrodynamic lubrication. Because the impeller is the greatest contributor to the load, the load is maintained at a minimum by scalloping the shroud of the impeller and employing pump out vanes or pump out slots. The scalloping reduces the amount of area that the pressure behind the shroud acts on. The slots or vanes reduce the pressure and also create the driving force of the flow throughout the path. Tests were conducted with various sizes and numbers of slots and vanes to obtain the optimum flow without consuming excessive horsepower.

The pressure at the hub of the impeller as a percentage of the impeller developed pressure is represented by k_h. This is a significant parameter that affects the calculation of the axial load on the impeller. Thus, tests were conducted on how k_h changed with changes in pump flow, impeller diameter, change in speed, and change in the peripheral shape of the impeller shroud.

The value of k_h does not follow the slope of the performance curve. This is because it is affected by the developed pressure within the volute and not the total pressure. As a result, the impeller load is almost constant with change in flow, with a downward slope toward higher flowrates. Thus, a higher axial load at flowrates above the best efficiency point is obtained than if the total developed pressure had been used (Guinzburg and Buse, 1995).

The axial load does not change as the fourth power with cut in impeller diameter, because the amount of scalloping of the back shroud is reduced as the impeller is cut. This increases k_h and results in a higher load. It was found that the load changes with the square of the impeller diameter.

The pressure at the hub does not change with the square of the speed, because the swirl generated by the pump out vanes or pump out slots and the return flow to the hub affect the pressure distribution on the shroud.

These values for k_h, as a function of impeller configuration obtained from experimental observation, are stored in the program database. The axial load is therefore predicted on the basis of the liquid characteristics along with the impeller configuration and speed of the pump. The load is given for flowrates that are 3

percent, 50 percent, 100 percent, and 120 percent of the best efficiency flowrate. Another feature is that the program can indicate whether the loading is due to boundary or hydrodynamic lubrication. A warning is given if the bearings are overloaded for that application.

From testing, the carrier contribution to the axial force was experimentally determined. Equation (3) is the contribution from the impeller only.

$$F_{impeller} \equiv [(C_A \cdot d^2 - d_s^2) \cdot (C_A + k_h) - (C_A \cdot d^2 - d_1^2) \cdot C_A] \cdot sg \cdot \frac{H}{2 \cdot 2.309} \cdot \frac{\pi}{4} \quad (3)$$

Experimentally determined coefficients of the pressure at the impeller back hub location are given in Table 3 for some typical pumps, in terms of k_h for various diameter cuts and flowrates as a percentage of BEP flow.

Table 3. K_h for a Typical Pump for Various Impeller Diameters and Pump Flows.

	$1 \geq d/d_2 > 0.87$	$.87 \geq d/d_2 > 0.8$	$.8 \geq d/d_2 > 0.65$
k_h (3%)	0.28	0.38	0.42
k_h (20%)	0.23	0.31	0.35
k_h (50%)	0.23	0.31	0.35
k_h (100%)	0.16	0.22	0.24
k_h (120%)	0.13	0.18	0.2

The pressure on the thrust collar is given by Equation (4) and the PV value is given by Equation (5).

$$P_{collar} \equiv \frac{F_{Axial}}{A} \quad (4)$$

$$PV \equiv P_{collar} \cdot d_m \cdot rpm \cdot \frac{60}{229} \quad (5)$$

Liquid Temperature Distribution

The temperature distribution in the liquid arising from the energy inputs at significant points along the flowpath must be determined in order to establish the corresponding vapor pressure values. Figure 9 defines these points.

Derivation of the Thrust Collar Temperature Rise

The most important step in bearing design is the determination of the operating regime of the bearing.

Full film lubrication is the term given to the condition whereby the sliding surfaces are separated by a full film of lubricant. The film thickness must be several times the surface roughness of the surface to prevent contact.

Also, as is more common in sealless pumps, the films can be self generating by favorable surface geometry and relative surface velocity. This is hydrodynamic lubrication.

The characterization of load versus film thickness can be made as follows (Shapiro, 1991):

$$w \equiv \frac{F_{Axial} 0.00025^2}{6 \cdot \mu \cdot 0.000000145 \cdot (rpm \cdot \frac{\pi}{30}) \cdot r_0^2} \quad (6)$$

where w is a dimensionless load parameter.

For $w > 0.0992$, the dimensionless film thickness t is given by:

$$t \equiv 0.06 \quad (7)$$

For $w <= 0.0992$, the dimensionless film thickness t is given by:

$$t \equiv \frac{0.0024}{w + 0.1008^2} \quad (8)$$

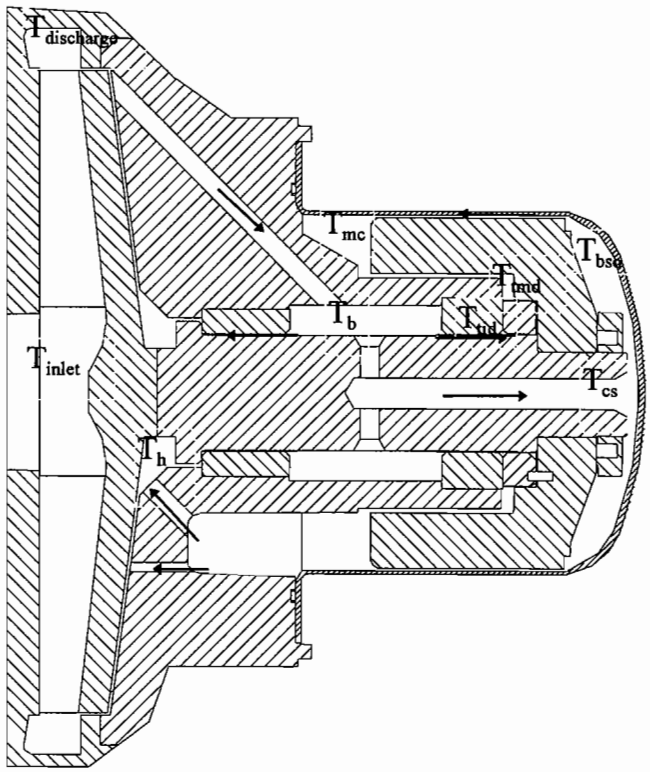

Figure 9. Internal Temperature Nomenclature.

For hydrodynamic lubrication, the shear stress is:

$$\iota \equiv d_m \cdot rpm \cdot \frac{0.0000308628}{t} \quad (9)$$

and the hydrodynamic lubrication load is:

$$L \equiv \iota \cdot A \quad (10)$$

On the other hand, the boundary lubrication load is:

$$L \equiv 0.03 \cdot F_{Axial} \quad (11)$$

The larger of these two loads is used in the calculation for the thrust collar temperature rise. The thrust collar temperature rise is found from the corresponding horsepower:

$$hp \equiv L \cdot \frac{d_m}{2} \cdot \frac{rpm}{63000} \quad (12)$$

Thus the temperature rise is:

$$\Delta T_{collar} \equiv \frac{5.1 \cdot hp}{Q_{bb} \cdot sg \cdot cp} \quad (13)$$

The temperature rise across the magnets is derived from the eddy current horsepower:

$$hp \equiv \delta HP \cdot (\frac{rpm}{3550})^2 \quad (14)$$

Hence, the temperature rise is as follows:

$$\Delta T_{magnet} \equiv \frac{C_M \cdot 5.1 \cdot hp}{Q_m \cdot sg \cdot cp} \quad (15)$$

From the results of measurements, the temperature between the bushings, the temperature at the ID of the thrust collar, the temperature at the center of the shell, and the temperature at the back of the shell at the OD of the magnet are assumed to be identical and equal to the temperature at the discharge flange

obtained by calculating a temperature rise of the liquid passing through the casing.

The temperature at the mean diameter of the thrust collar is given by:

$$T_{tmd} \equiv T_{bb} + \Delta T_{collar} \tag{16}$$

And the temperature rise across magnets is:

$$\Delta T_m \equiv \frac{\Delta T_{magnet} \cdot Q_m + \Delta T_{collar} \cdot [Q_{bb} - (Q_m - Q_s)]}{Q_{bb} + Q_m} \tag{17}$$

The temperature at the impeller hub is related to the discharge temperature through an energy balance of the fluid from the magnet chamber mixing with the fluid from between the bearings as follows:

$$T_h \equiv T_{discharge} + \Delta T_h \tag{18}$$

PROGRAM INPUT AND OUTPUT

The user enters a limited amount of information that includes the particular pump selection and fluid properties:

- Pump size
- rpm
- gpm
- Impeller diameter
- Inlet pressure expressed as NPSH
- Operating temperature
- Vapor pressure at operating temperature
- Vapor pressure at two other temperatures to characterize the fluid
- Specific gravity
- Viscosity
- Specific heat

Other information such as geometrical dimensions and performance data have been stored in the program database. Data are stored as either specific to the frame (model) size or more specific to the particular pump size. For each frame (model), constants are stored in the program so that the user does not have to enter them each time. The input screen for the program is shown in Figure 10. Because the program has been developed for worldwide use, the terminology can be selected in *Metric Mode* or in *Customary US Mode*.

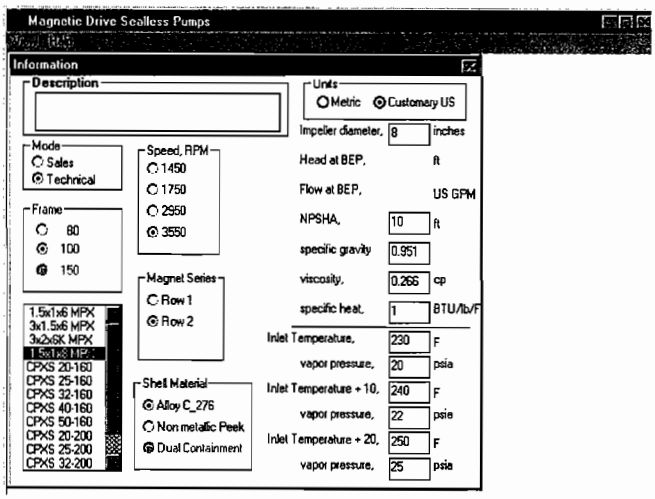

Figure 10. Input Screen for the Flowpath Program.

When the user has selected the conditions for analyzing the lubrication flow inside the magnetic drive pump, the results can be examined as a graphical output. In Figure 11, the flows resulting from the input conditions given in Figure 10 are shown. The pressure distribution is shown in Figure 12. Alongside the pressures, the vapor pressures for the given temperature at the specified location are also given. Should the vapor pressure be within 10 percent of the pressure, a *warning signal* is shown to alert the user of the possibility of flashing. In Figure 13, the temperature distribution is shown. The user may obtain printouts from 1 to 15 selected points as shown in figure 14.

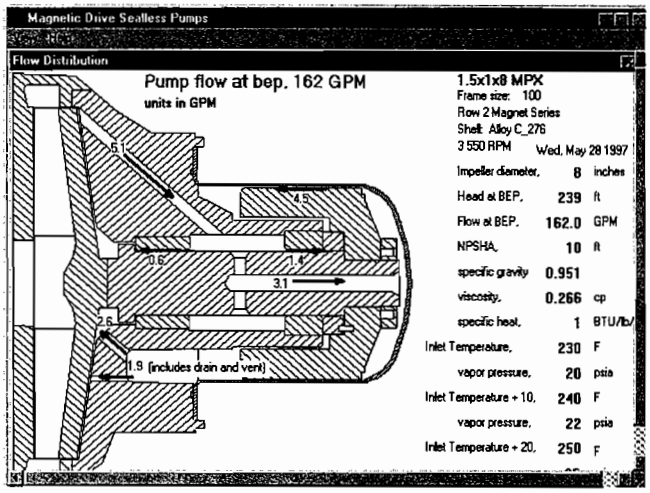

Figure 11. Flow Distribution of the Lubrication Path for the Conditions Listed in Figure 10.

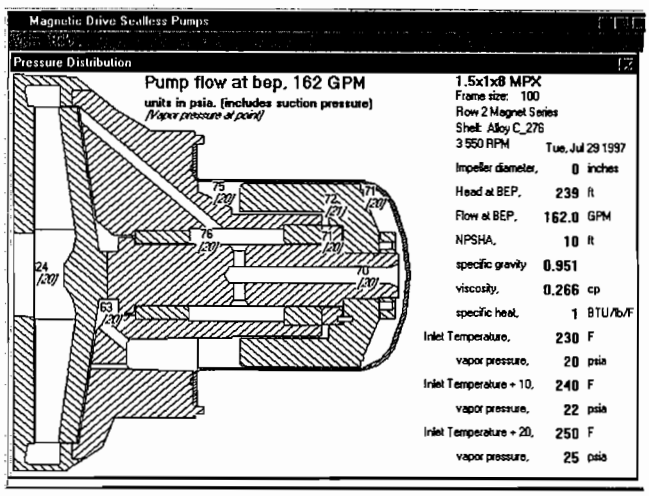

Figure 12. Pressure Distribution of the Lubrication Path for the Conditions Listed in Figure 10.

APPLICATION LIMITATIONS

When the pressure along the flowpath is within dangerous proximity to the vapor pressure, a warning is displayed. The axial loading on the thrust collar is also limited and an error message is produced when this value is exceeded.

In addition, the following inputs are checked for correctness:

- If the impeller cut specified is less than the minimum percentage of the maximum impeller OD, as published in the price book curves, then a message is issued and the user is forced to select another pump size.

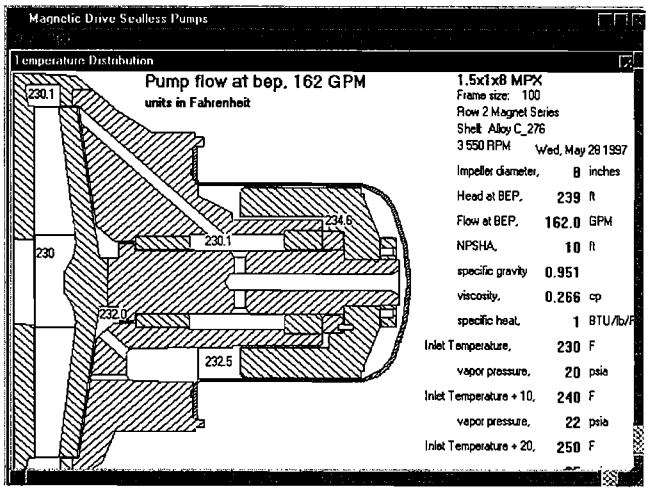

Figure 13. Temperature Distribution of the Lubrication Path for the Conditions Listed in Figure 10.

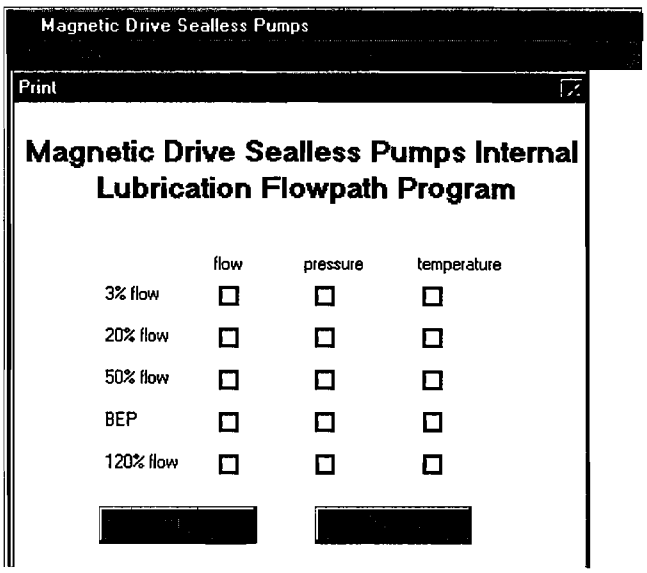

Figure 14. Print Selection Screen for Conditions at Various Flowrates.

- An error message is also generated if the user attempts to use an impeller diameter that is greater than the size of the maximum impeller OD.
- The program does not handle any viscosities greater than 260 cp, and any value above this is rejected.

CONCLUSIONS

A computer program that utilizes graphical user interfaces was designed to analyze the internal flow system in a magnetically driven sealless chemical pump, which employs high torque rare-earth magnets. The pumps for which this simulation was developed have a semiopen impeller in an end suction single volute.

The program is a result of both theoretical and test work. The testing involved a wide range of pump sizes. Within each size, an extensive matrix involved running at different speeds, different cut impeller diameters, and from shutoff through runout conditions. Measurements of pressure, temperature, and flow were obtained for each individual flowpath within the lubrication system. The results for each passage within the flowpath were then compared with analytical predictions. These results have been used to generate the database for the program, which simulates the flowpath in the lubrication system of a magnetically driven pump.

The computer simulation predicts the flows, pressures, and temperatures of individual flowpaths, along with the axial load, by taking into account the effects of viscosity, vapor pressure, and other liquid properties on the local pressures in the pump. In order to examine the operation of the pump in the user's particular fluid, the flow is simulated in the program using a graphical user interface. A graphical output is given of all the pertinent locations in the system, such as the thrust collar face. This is of particular concern with low specific heat volatile liquids. With these liquids, it is crucial to be able to predict flashing, since this could produce premature pump failure.

NOMENCLATURE

A = area of the thrust collar, in^2
BEP = best efficiency point
BHP_{BEP} = brake horsepower at the best efficiency point at 3550 rpm, hp
BHP_{so} = brake horsepower of the pump at shutoff
C_A = axial factor, which depends on the percent cut diameter
C_M = empirical factor, which depends on the type of shell
c_h = viscosity correction to pressure, from Hydraulic Institute Standards (HI)
c_q = viscosity correction to flow, from HI
c_η = viscosity correction to efficiency, from HI
d = impeller diameter, in
d_1 = impeller inlet diameter, in
d_2 = maximum impeller exit diameter, in
d_s = shaft diameter, in
d_m = mean diameter of thrust bushing, in
F_{axial} = axial load, lb
g = acceleration due to gravity, ft/sec^2
H = developed head, $u^2/2g$, ft
k_h = experimentally determined coefficient of static head at the impeller hub
L = load on axial thrust bearing, lb
P = developed pressure, psi
P_{bb} = pressure between the bushings
P_{tod} = pressure at the OD of the thrust collar
P_{mc} = pressure in the magnet chamber
P_h = pressure at the impeller hub
P_{cs} = pressure at the centerline of the shaft at the shell end
P_{bso} = pressure at the back of the shell at the OD of the magnet
P_{tid} = pressure at the ID of the thrust collar
Q = flow in gpm
Q_f = injection to the flowpath
Q_{fb} = flow through the front bushing
Q_{vd} = flow through the vent and drain
Q_h = flow through the hub return
Q_m = flow across the magnets
Q_s = flow through the shaft
Q_{bb} = flow through the back bushing
r_0 = outside radius of thrust collar, in
t = dimensionless film thickness (Shapiro, 1991)
u = impeller tip speed at the cut diameter, ft/sec
w = dimensionless axial load (Equation (6))
WP = effective weight of metal parts of pump, lb
sg = specific gravity
V = volume of liquid contained in the volute, gal
δHP = horsepower consumption due to eddy currents
η = efficiency at cut impeller diameter
μ = dynamic viscosity, cp
ν = kinematic viscosity, cs
ι = shear stress on fluid in axial thrust bearing, psi

REFERENCES

Buse, F. W. and Stoughton, C. D., 1990, "Design of Magnetically Driven Chemical Pump to Fit ANSI B73.1 Dimensions Using a Semiopen Impeller," *Proceedings of the Seventh International Pump Users Symposium*, Turbomachinery Laboratory, Texas A&M University, College Station, Texas, pp. 55-62.

Guinzburg, A. and Buse, F. W., 1995, "Magnetic Bearings as an Impeller Force Measurement Technique," *Proceedings of the Twelfth International Pump Users Symposium*, Turbomachinery Laboratory, Texas A&M University, College Station, Texas, pp. 69-76.

Heald, C. C., Behnke, P. W., and Gussert, R. F., 1992, "Development and Qualification of a Magnetically Coupled Process Pump for API 610 7th Edition Services," *Proceedings of the Ninth International Pump Users Symposium*, Turbomachinery Laboratory, Texas A&M University, College Station, Texas, pp. 9-21.

Hernandez, T., 1991, "A User's Engineering Review of Sealless Pump Design Limitations and Features," *Proceedings of the Eighth International Pump Users Symposium*, Turbomachinery Laboratory, Texas A&M University, College Station, Texas, pp. 129-145.

Mayes, J. D., 1990, "Magnetically Driven Centrifugal Pumps—Eliminating Seal Problems in Refinery and Chemical Processing Plant Equipment," *Proceedings of the Seventh International Pump Users Symposium*, Turbomachinery Laboratory, Texas A&M University, College Station, Texas, pp. 93-100.

Schommer, H. J. and Johnson, T., 1990, "Design, Construction, and Application of Magnetically Coupled Centrifugal Pumps," *Proceedings of the Seventh International Pump Users Symposium*, Turbomachinery Laboratory, Texas A&M University, College Station, Texas, pp. 63-71.

Shapiro, W., April 1991, "Analysis of "Magnoseal" Pump Bearing," MTI 91TR30 Mechanical Technologies Inc. Internal Report.

BIBLIOGRAPHY

Eierman, R. G., 1990, "A User's View of Sealless Pumps—Their Economics, Reliability and the Environment," *Proceedings of the Seventh International Pump Users Symposium*, Turbomachinery Laboratory, Texas A&M University, College Station, Texas, pp. 127-134.

ACKNOWLEDGEMENTS

The authors wish to thank the management of Ingersoll-Dresser Pump Company for permission to publish this paper. Special thanks is extended to Paul Cooper of the Research and Development Department. The authors are especially grateful to Azfar Ali of the Research and Development Department, John Dodson of the plant in Newark, and Jim Allen of the Chesapeake plant who cheerfully helped to debug the computer program.